nature communications

Article

https://doi.org/10.1038/s41467-024-52071-5

A robust mouse model of HPIV-3 infection and efficacy of GS-441524 against virus-induced lung pathology

Received: 18 April 2024

Accepted: 22 August 2024

Published online: 05 September 2024

Check for updates

Yuxia Lin[1], Mona Khan[2], Birgit Weynand[3], Manon Laporte[1], Frank Coenjaerts[4], Darius Babusis[5], John P. Bilello[5], Peter Mombaerts[2], Dirk Jochmans[1] & Johan Neyts[1,6]

Human parainfluenza virus type 3 (HPIV-3) can cause severe respiratory tract infections. There are no convenient small-animal infection models. Here, we show viral replication in the upper and lower airways of AG129 mice (double IFNα/β and IFNγ receptor knockout mice) upon intranasal inoculation. By multiplex fluorescence RNAscope and immunohistochemistry followed by confocal microscopy, we demonstrate viral tropism to ciliated cells and club cells of the bronchiolar epithelium. HPIV-3 causes a marked lung pathology. No virus transmission of the virus was observed by cohousing HPIV-3-infected AG129 mice with other mice. Oral treatment with GS-441524, the parent nucleoside of remdesivir, reduced infectious virus titers in the lung, with a relatively normal histology. Intranasal treatment also affords an antiviral effect. Thus, AG129 mice serve as a robust preclinical model for developing therapeutic and prophylactic strategies against HPIV-3. We suggest further investigation of GS-441524 and its prodrug forms to treat HPIV-3 infection in humans.

Human parainfluenza viruses (HPIVs, family *Paramyxoviridae*) are highly transmissible viruses that are responsible for common acute respiratory infections, ranging from colds and croup to bronchiolitis and pneumonia across all age groups, with the highest infection rate observed in young children[1,2]. Of the four HPIV serotypes, HPIV-3 is the most virulent, primarily causing lower respiratory tract illnesses such as bronchiolitis and pneumonia, particularly in children under 5 years[3,4]. HPIV-3 infection is an important cause of morbidity and mortality in immunocompromised individuals and the elderly[5]. There are no vaccines for the prevention, nor antiviral drugs for the treatment of HPIV infections. Akin to other paramyxoviruses, HPIVs are single-stranded, negative-sense RNA viruses and encode six essential proteins: nucleocapsid protein (NP), phosphoprotein (P), matrix protein (M), fusion glycoprotein (F), hemagglutinin-neuraminidase (HN), and RNA-dependent-RNA polymerase (L).

BALB/c mice have been used in various HPIV-3 studies to assess immune responses to protein subunit vaccines[6,7]. No robust HPIV-3 challenge models have been reported for immunocompetent mice, suggesting that they are not or not sufficiently susceptible to HPIV-3. Infection models for HPIV-3 have been described in hamsters, guinea pigs, cotton rats, ferrets, sheep, and non-human primates[5,8,9]. Infection of hamsters results in low-level replication and mild bronchiolitis[10]; this model has been used occasionally. In cotton rats the virus replicates in the nasal turbinates and lungs; this model has been used in a few studies to assess the efficacy of antiviral drugs and vaccine candidates[11–14]. In ferrets intranasal infection leads to

[1]KU Leuven Department of Microbiology, Immunology and Transplantation, Rega Institute for Medical Research, Virology, Antiviral Drug & Vaccine Research Group, Leuven, Belgium. [2]Max Planck Research Unit for Neurogenetics, Frankfurt, Germany. [3]KU Leuven Department of Imaging and Pathology, Division of Translational Cell and Tissue Research, Leuven, Belgium. [4]Department of Medical Microbiology, University Medical Center Utrecht, Utrecht University, Utrecht, The Netherlands. [5]Gilead Sciences Incorporated, Foster City, CA, USA. [6]VirusBank Platform, KU Leuven, Leuven, Belgium.
e-mail: johan.neyts@kuleuven.be

replication in the lower airways and limited replication in the upper airways; no overt histological lesions were observed in the putative target cells[15]. A few older studies report hypersensitivity of the airways upon infection of guinea pigs[16–18]. African green monkeys and newborn lambs also allow for viral replication, and bronchointerstitial pneumonia was noted in lambs[9,19]. The non-human primate and newborn lamb models have been used for studies of vaccine candidates[9,20–22]. Taken together, there are no robust HPIV-3 infection models in mice, hamsters or guinea pigs. The virus replicates well in the respiratory tract of cotton rats, ferrets, lambs, and African green monkeys, but these species are much less convenient as preclinical models than mice because of their larger body size, higher cost, limited availability, and more complex handling and husbandry. Moreover, these species are not inbred so the findings may be less reproducible due to differences in genetics.

Here, we set out to develop an inbred mouse HPIV-3 infection model for prophylactic and therapeutic modalities. The AG129 strain is a widely available inbred 129/Sv strain that carries a double knockout in receptor genes for IFNα/β and IFNγ[23] and supports the replication of several viruses[24–26]. We show that AG129 mice support viral replication of HPIV-3 and develop bronchopneumonia and hyperplasia of pneumocytes upon intranasal inoculation. Using GS-441524, the parent nucleoside of remdesivir[27], we validated this model for antiviral studies.

Results

Replication potential of HPIV-3 in various mouse strains upon intranasal inoculation

In preliminary experiments, we explored whether intranasal inoculation of five inbred mouse strains results in measurable viral replication: BALB/c, SCID, C57BL/6, Ifnar−/−, and AG129. Mice ($n = 4$ per strain) were intranasally inoculated with 1.5×10^6 50% tissue culture infective doses ($TCID_{50}$) of HPIV-3. Mice were killed at days 1, 3, 7, or 10 post-infection (p.i.), and viral loads in the lung were determined (Fig. S1a). Infectious virus titers in the lung of all BALB/c, SCID, C57BL/6, and Ifnar−/− mice remained below 2 $\log_{10}$ $TCID_{50}$/mg lung sample at any time point (Fig. S1b, data not shown for BALB/c and SCID mice). In contrast, in AG129 mice, median infectious virus titers at day 1 p.i. were 2.9 $\log_{10}$ $TCID_{50}$/mg lung sample (Fig. S1b). There was a minor gain in body weight of C57BL/6, Ifnar−/−, and AG129 mice (Fig. S1c). Histological examination with hematoxylin-eosin (H&E) staining of C57BL/6 mice revealed minimal lung pathology. In Ifnar−/− mice, peribronchial inflammation and perivascular inflammation were detected in the lung from day 7 p.i. and the severity increased until day 10 p.i., the end of the experiment. In AG129 mice, the first pathological changes, with very limited focal areas of peribronchial inflammation, were observed as early as day 1 p.i., and these increased over time to bronchopneumonia and hyperplasia of pneumocytes, with median cumulative lung pathology scores of 4.0 at day 7 p.i. (Fig. S1d). Based on these results, we decided to further explore AG129 mice as a model for HPIV-3 infection.

Kinetics of HPIV-3 replication in AG129 mice

Next, we infected AG129 mice intranasally with HPIV-3 and collected lung samples and nasal-pharyngeal-laryngeal-tracheal washes (NPLT-washes) at 0.5 h, 6 h, 1 day, 2 days, 3 days, 5 days, and 7 days p.i. to quantify infectious virus titers in the lung and NPLT-washes (Fig. 1a). Infectious virus titers in the lung peaked at day 1 p.i. (median value of 3.2 $\log_{10}$ $TCID_{50}$/mg lung sample), followed by a gradual decrease from day 2 p.i. (median values of 2.5, 2.2, and 1.1 $\log_{10}$ $TCID_{50}$/mg tissue) to undetectable levels at day 7 p.i. (Fig. 1b). Infectious virus titers in NPLT-washes persisted from day 1 to day 5 p.i. (~3.7 $\log_{10}$ $TCID_{50}$/mL) and sharply declined to undetectable levels at day 7 p.i. (Fig. 1c). Infected mice did not present with overt changes in alertness or physical activity, except for a minor weight change at days 5 and 7 p.i. (Fig. 1d). Histological examination revealed focal areas of peribronchial inflammation in the lung at day 3 p.i. Pathological changes developed prominently from day 5 p.i., a time point at which viral replication was declining. At day 7 p.i., the lung parenchyma was severely affected, with substantial perivascular and peribronchial inflammation and hyperplasia of pneumocytes across the entire area (Fig. S2). Median histopathology scores at days 5 and 7 p.i. were 4.3 and 4.0, respectively (Fig. 1e). Taken together, we demonstrated that AG129 mice support sufficient viral replication and develop lung pathology upon intranasal inoculation of HPIV-3.

Tropism of HPIV-3 to ciliated cells and club cells of the bronchiolar epithelium

HPIV-3 is a single-stranded negative-sense RNA virus. To determine the target cell types—the cellular tropism—in AG129 mice, we performed confocal imaging of sections stained in multiplex with the RNAscope technology, which visualizes a single RNA molecule as a dot or "punctum," plural "puncta"[28], combined with immunohistochemistry (IHC), which visualizes an antigen as an immunoreactive (IR) signal. The precision of confocal imaging supports the robust characterization of a cell type or an individual cell as a target cell type or infected cell, respectively. We adopted the same workflow as we developed previously for postmortem samples of COVID-19 patients to visualize the patterns of infection with SARS-CoV-2, a single-stranded positive-sense RNA virus[29–33].

At the level of the lung, the respiratory tract consists mostly of bronchioles terminating in alveoli (Fig. 2). Most cells in the bronchiolar epithelium contain Krt8-IR signal. Major cell types in the bronchiolar epithelium are ciliated cells and club cells. An RNAscope probe for the gene *Foxj1*, encoding a transcription factor that is required for ciliogenesis, identifies ciliated cells (Fig. 2a). An RNAscope probe for the gene *Scgb1a1*, encoding an antimicrobial secretory protein that is also referred to as CC10, uteroglobin, or blastokinin, identifies club cells (Fig. 2a). The alveolar wall contains type I pneumocytes, which can be identified with an RNAscope probe for *Ager*, encoding a receptor for advanced glycosylation end products. Type II pneumocytes can be identified with an RNAscope probe for *Sftpc*, encoding surfactant associated protein C (Fig. 2a, j–l).

As expected, sections through lung samples of uninfected mice did not yield RNAscope puncta for the viral hemagglutinin-neuraminidase gene *HPIV-3-HN* (Fig. 2b) nor for the viral nucleocapsid gene *HPIV-3-NP* (Fig. 2c). At day 1 p.i. (Fig. 2d, e) and day 3 p.i. (Fig. 2g–i), numerous ciliated cells and club cells harbored densely packed *HPIV-3-HN* and *HPIV-3-NP* puncta, colocalizing in the same cells. By contrast, at day 10 p.i., a small fraction of cells in the bronchiolar epithelium harbored *HPIV-3-NP* puncta (Fig. 2f). In the alveoli at day 5 p.i., neither cells harboring *Ager* puncta (Fig. 2j, k) nor cells harboring *Sftpc* puncta (Fig. 2l) harbored *HPIV-3-NP* puncta. Roundish cells were densely packed with *HPIV-3-NP* puncta and may represent intra-alveolar histiocytes (Fig. 2j–l).

Taken together, confocal imaging of sections subjected to multiplex fluorescence staining with the ultrasensitive RNAscope platform for RNA in situ hybridization combined with IHC enabled us to assign HPIV-3 tropism in AG129 mice to ciliated cells and club cells of the bronchiolar epithelium. We did not uncover evidence for tropism to type I or type II pneumocytes in the alveolar wall, but the absence of evidence does not equal the evidence of absence.

Prophylactic oral treatment of GS-441524 reduces viral loads and lung pathology

We reasoned that, if the infectious viruses detected in the lung reflected active replication, it should be possible to suppress viral replication by treatment with an inhibitor of HPIV-3 replication. We opted for GS-441524, the parent nucleoside of remdesivir (Veklury, Gilead Sciences), a drug that has been approved for the treatment of

https://doi.org/10.1038/s41467-024-52071-5

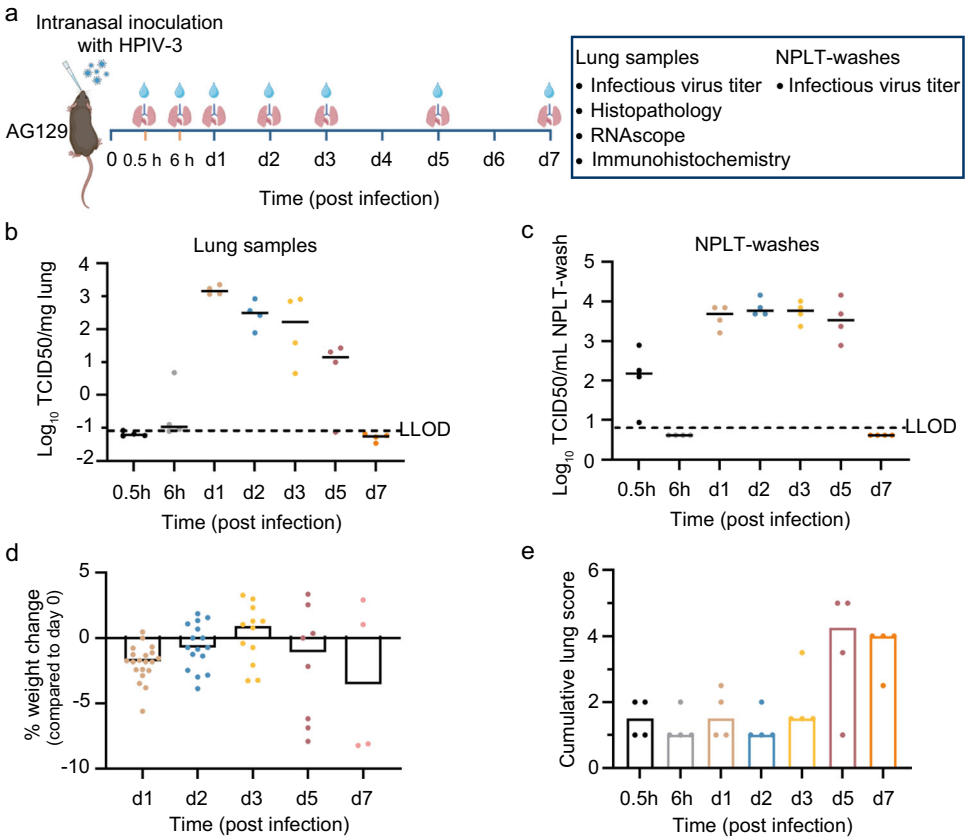

Fig. 1 | Kinetics of HPIV-3 replication in intranasally inoculated AG129 mice. **a** Setup of the study. AG129 mice were intranasally inoculated with 1.5×10^6 $TCID_{50}$ of HPIV-3. Lung samples and NPLT-washes were collected at various time points post-infection (p.i.). **b** Infectious virus titers are expressed as log_{10} $TCID_{50}$ per milligram of lung sample. **c** Infectious virus titers are expressed as log_{10} $TCID_{50}$ per milliliter of NPLT-wash. **d** Weight change at various time points post-infection is presented as a percentage of the body weight at the time of inoculation. **e** Cumulative severity scores of lungs of all infected mice. Individual data and median values (indicated by bars) are presented in all graphs. LLOD presents the lower limit of detection. Data are from one experiment with four mice per group. Source data are provided as a Source Data file. **a** was designed with BioRender.

COVID-19[34]. GS-441524 is intracellularly phosphorylated to the 5′-triphospate that inhibits the viral RNA-dependent RNA polymerase[27]. GS-441524 and remdesivir inhibit the in vitro replication of parainfluenza viruses and other paramyxoviruses[35]. AG129 mice were orally treated twice daily (BID) with vehicle or GS-441524 (50 mg/kg), starting 1 day before intranasal inoculation of HPIV-3. Treatment was continued for four consecutive days (Fig. 3a). As we had observed high viral titers in untreated mice at day 3 p.i. (Fig. 1), this timepoint was set as the endpoint for the treatment experiment. There was no weight loss or any clinical sign of adverse effects in either group (Fig. S3a). GS-441524 treatment led to a reduction of 3.1 log_{10} $TCID_{50}$/mg lung sample ($p < 0.0001$) of infectious virus titer and a reduction of 1.3 log_{10} $TCID_{50}$ equivalent/mg lung sample ($p < 0.0001$) of HPIV-3 RNA in the lung compared to the vehicle-treated group (Fig. 3b, c). No or only very limited infectious virus titers were detected in the GS-441524-treated animals (Fig. 3b). In contrast, no difference in infectious virus titers and HPIV-3 RNA in NPLT-washes was observed between the GS-441524-treated and the vehicle-treated groups (Fig. S3b, c).

Considering the kinetics of HPIV-3 replication and the late development of lung histopathology (day 5 p.i.), we conducted another experiment with the same setup but whereby lung samples were collected at day 6 p.i. to assess the impact of antiviral treatment on lung pathology (Fig. 3d). There was no weight loss or any clinical sign of adverse effects in either group at day 6 p.i. (Fig. 3e). The lungs of uninfected mice appeared normal. The lungs of the vehicle-treated group displayed inflammation, primarily in the centrilobular regions, accompanied by bronchopneumonia, perivascular inflammation, and peribronchial inflammation. In contrast, in GS-441524-treated mice only very focal and limited perivascular inflammation was noted within the nearly normal lung parenchyma (Fig. 3f). The median lung histopathology score in the vehicle-treated animals was 4.5 versus 1.5 in the GS-441524-treated mice ($p = 0.0002$) (Fig. 3g). Taken together, we demonstrated that oral treatment of GS-441524 significantly reduces viral loads and pathology in the lung of HPIV-3-infected AG129 mice.

A viral RNA species reflecting ongoing viral replication is drastically reduced in the target cell types of the bronchiolar epithelium by treatment with GS-441524

Our data on infectious virus titers of lung samples indicated that viral loads in the target cell types are affected by GS-441524 but do not provide information on the sites of inhibition of viral replication. We therefore performed confocal imaging of sections subjected to multiplex fluorescence staining with RNAscope and IHC (Fig. 4). Antigenome RNA species are not present in virions of this single-stranded, negative-sense RNA virus, but are transiently produced during the viral life cycle such that their presence reflects ongoing viral replication within target cells. We custom-designed an RNAscope *HPIV-3-NP-sense* probe, which we here refer to as the *HPIV-3-NP-antigenome* probe as a more intuitive reference to the virological significance of the puncta revealed by this probe.

As expected, a section through a lung sample of an uninfected mouse did not yield RNAscope puncta for the *HPIV-3-NP-antigenome* probe (Fig. 4a). In vehicle-treated mice (Fig. 4b–f), a major fraction of cells harboring *Foxj1* puncta (ciliated cells) or *Scgb1a1* puncta (club cells) also harbored *HPIV-3-NP-antigenome* or *HPIV-3-HN* puncta. Interestingly, *HPIV-3-NP-antigenome* puncta resided perinuclear

https://doi.org/10.1038/s41467-024-52071-5

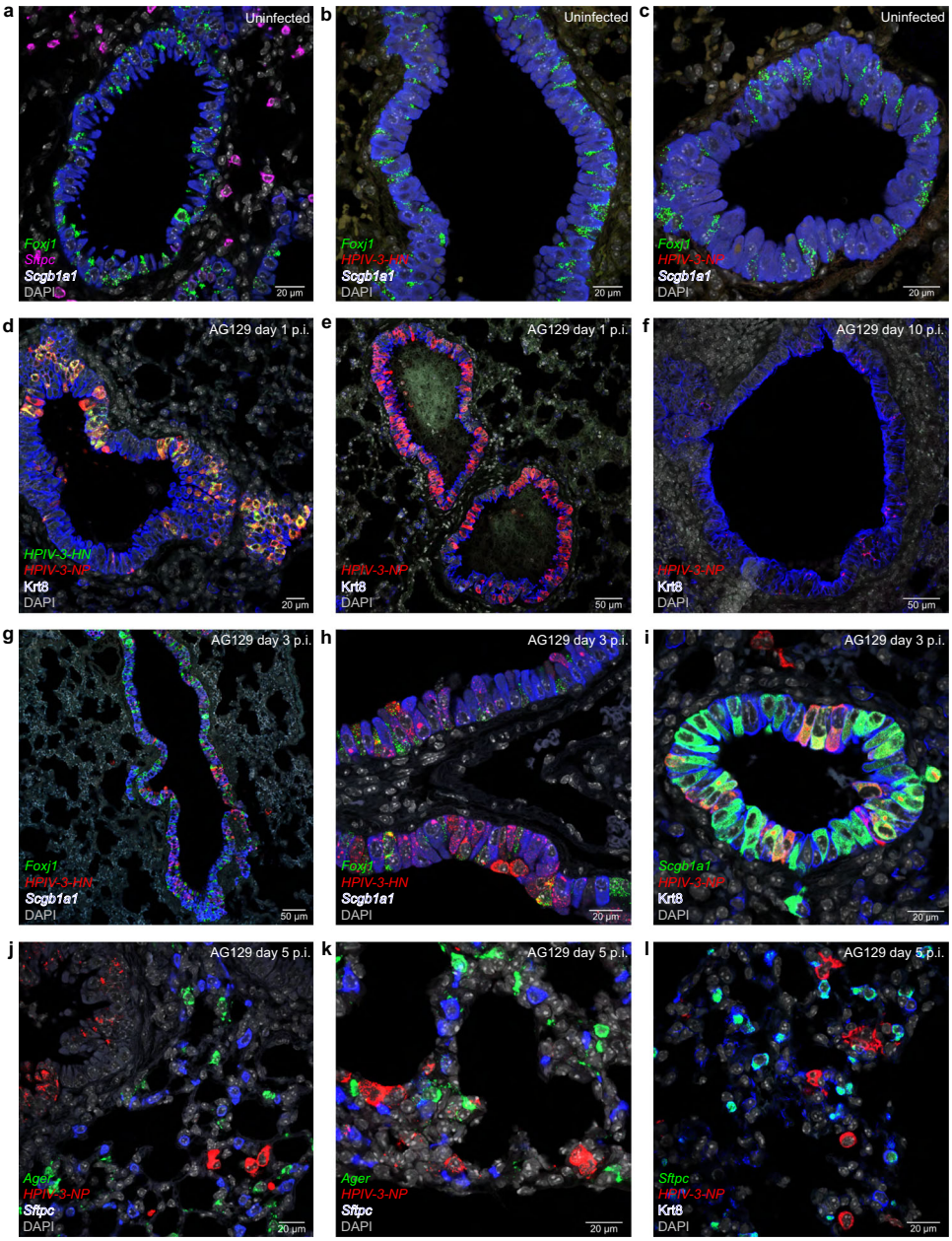

Fig. 2 | Tropism of HPIV-3 to ciliated cells and club cells of the bronchiolar epithelium of AG129 mice. Confocal images of 5 µm sections through lung samples. Multiplex fluorescence with RNAscope and IHC. The name of the mouse gene or viral RNA that is the target for an RNAscope probe, yielding puncta, is in italics. The name of the protein that is the target for an antibody, yielding an immunoreactive (IR) signal, is in roman. DAPI serves as a nuclear stain. **a**–**c** Uninfected, **d**, **e** 1 d.p.i., **f** 10 d.p.i., **g**–**i** 3 d.p.i., **j**–**l** 5 d.p.i. **a** Transverse section through a bronchiole. The lumen of the bronchiole (the black space at the center) is devoid of cells. Alveoli of the lung parenchyma surround the bronchiole. *Foxj1* is a marker for ciliated cells and *Scgb1a1* for club cells in the bronchiolar epithelium. *Sftpc* is a marker for type II pneumocytes in the alveolar wall. **b**, **c** As expected, there are no puncta for the *HPIV-3-HN* probe and the *HPIV-3-NP* probe in uninfected mice. **d** The Krt8-IR signal labels most epithelial cells in the bronchiolar epithelium. A fraction of the cells in the bronchiolar epithelium harbor *HPIV-3-HN* puncta and *HPIV-3-NP* puncta, colocalizing within the same cells. There are no such puncta in the alveoli surrounding the bronchiole. **e** Nearly all cells in the bronchiolar epithelium harbor *HPIV-3-NP* puncta. There are no such puncta in the alveoli surrounding the bronchiole. **f** A few cells in the bronchiolar epithelium harbor *HPIV-3-NP* puncta at this late endpoint, 10 d.p.i. **g**, **h** Triple RNAscope reveals *HPIV-3-HN* puncta colocalizing with *Foxj1* puncta or *Scgb1a1* puncta. **h** A fraction of the cells harboring *Foxj1* puncta or *Scgb1a1* puncta also harbor *HPIV-3-HN* puncta. **i** A fraction of the cells harboring *Scgb1a1* puncta also harbor *HPIV-3-NP* puncta. **j**–**l** These fields of view comprise only alveoli. *Ager* is a marker for type I pneumocytes. Roundish cells harbor densely packed *HPIV-3-NP* puncta but neither *Ager* puncta nor *Sftpc* puncta. The epithelium is referred to as bronchiolar epithelium, as the sections were made through parts of the lungs that are located peripherally. Numbers of biological replicates: **a**, $n = 1$; **b**, **c**, $n = 2$; **d**–**l**, $n = 3$.

(around the nucleus), whereas *HPIV-3-HN* puncta diffusely filled the cells (Fig. 4b). We previously reported a similar perinuclear location of *SARS-CoV-2-sense* puncta, representing antigenome RNA[30,31]. In sharp contrast, there were few (Fig. 4g, h) if any (Fig. 4i) *HPIV-3-NP-antigenome* or *HPIV-3-HN* puncta in sections through lung samples of GS-441524-treated mice. Taken together, by visualizing RNA species that reflect ongoing viral replication within target cells, we demonstrated that GS-441524 effectively reduces viral replication within the target cells of HPIV-3 in the bronchiolar epithelium—ciliated cells and club cells.

https://doi.org/10.1038/s41467-024-52071-5

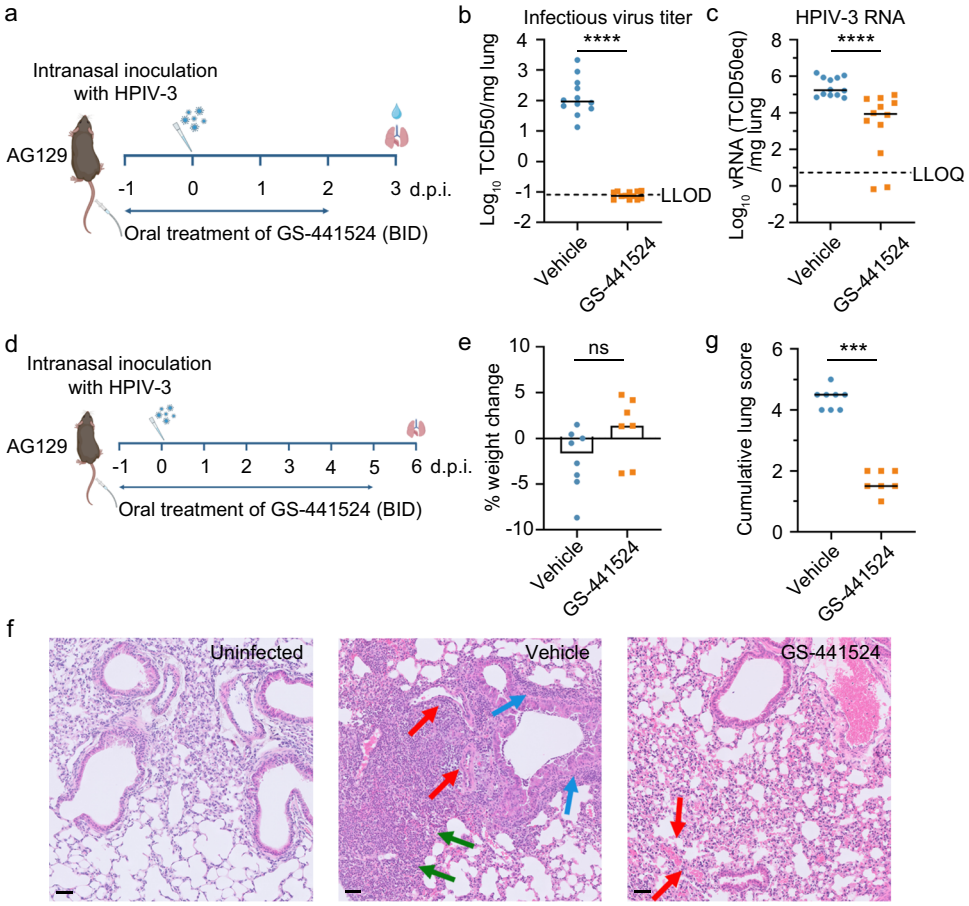

Fig. 3 | Prophylactic oral treatment with GS-441524 of AG129 mice intranasally inoculated with HPIV3 reduces viral loads and lung pathology. a Setup of the study. AG129 mice were orally treated twice daily with either vehicle or 50 mg/kg GS-441524 from day −1 p.i. to day 2 p.i., and intranasally inoculated with 1.5×10^6 $TCID_{50}$ of HPIV-3 at day 0 p.i. Lung samples were collected at day 3 p.i. to measure viral loads. **b** Infectious virus titers are expressed as log_{10} $TCID_{50}$ per milligram of lung sample. LLOD presents the lower limit of detection. **c** HPIV-3 RNA levels are expressed as log_{10} $TCID_{50}$ equivalent per milligram of lung sample. LLOQ presents the lower limit of quantification. **b**, **c** Data are from two independent experiments, each with 6 mice per group. Data were analyzed by the two-tailed Mann−Whitney *U* test. ****$p < 0.0001$. **d** Setup of the study. AG129 mice were orally treated twice daily with vehicle or 50 mg/kg GS-441524 from day −1 p.i. to day 5 p.i., and intranasally inoculated with 1.5×10^6 $TCID_{50}$ of HPIV-3 at day 0 p.i. Lungs were collected at day 6 p.i. for lung histopathology assessment. **e** Weight change at day 6 p.i. is presented as a percentage of the body weight at day −1 p.i., when treatment was started. **f** Representative H&E-stained images reveal normal lung parenchyma in uninfected mice, centrilobular accentuation of inflammation with bronchopneumonia (green arrows), perivascular inflammation (red arrows), and peribronchial inflammation (blue arrows) in the vehicle-treated mice, and very focal and limited perivascular inflammation (red arrows) in the GS-441524-treated mice. The scale bar is 50 μm. The samples of uninfected mice and infected mice were from the same experiment, but the staining procedure was performed at different moments. **g** Cumulative severity scores of lungs of all infected mice. **e**, **g** Data are from one experiment with 8 mice in the vehicle-treated group and 7 mice in the GS-441524-treated group. Data were analyzed with the two-tailed Mann−Whitney *U* test. ns nonsignificant, ***$p = 0.0002$. Individual data and median values (indicated by bars) are presented in all graphs. Source data are provided as a Source Data file. **a**, **d** were designed with BioRender.

Intranasal treatment of GS-441524 reduces viral loads and lung pathology

Since oral treatment of GS-441524 did not appear to reduce viral loads in NPLT-washes, we next explored whether intranasal treatment of GS-441524 would be able to do so. AG129 mice were intranasally treated once daily with GS-441524 (40 μL/mouse of a 30 mg/mL solution), starting 1 day before intranasal inoculation of HPIV-3. Mice were killed at day 3 p.i. and lung samples and NPLT-washes were collected (Fig. 5a). GS-441524 treatment reduced infectious virus titers by 2.3 log_{10} $TCID_{50}$/mg lung sample ($p = 0.0048$) and HPIV-3 RNA by 1.1 log_{10} $TCID_{50}$ equivalent/mg lung sample ($p = 0.0071$) compared to the vehicle-treated group (Fig. 5b, c). Interestingly, intranasal treatment with GS-441524 reduced infectious viral titers by 1.4 log_{10} $TCID_{50}$/mL ($p < 0.0001$) and HPIV-3 RNA by 1.1 log_{10} $TCID_{50}$ equivalent/mL ($p < 0.0001$) in NPLT-washes compared to the vehicle-treated group (Fig. 5d, e).

To assess the effect of intranasal treatment on lung pathology, lungs were collected at day 6 p.i. (Fig. 5f) using the same experimental setup. There is no significant difference in weight change between the two groups (Fig. 5g) and no clinical signs of adverse effects. In vehicle-treated mice, the lung exhibited perivascular inflammation, peribronchial inflammation, and hyperplasia of pneumocytes. In contrast, GS-441524 treatment significantly reduced lung pathology, with only a small area of bronchopneumonia, perivascular inflammation, and some hyperplasia of pneumocytes in the centrilobular regions (Fig. 5h). The median lung pathology score in vehicle-treated animals was 3.0 in GS-441524-treated mice, compared to 5.0 in vehicle-treated mice ($p = 0.0070$) (Fig. 5i).

A single intranasal prophylactic dose of GS-441524 inhibits HPIV-3 replication in the lung

Next, AG129 mice were treated prophylactically with a single intranasal dose of GS-441524 (40 μL/mouse of a 30 mg/mL solution) either at 6 h or 1 h before intranasal inoculation, and lungs were collected at day 3 p.i. (Fig. 6a). Prophylaxis with GS-441524 resulted in reductions of 0.8 log_{10} $TCID_{50}$/mg lung sample ($p = 0.0390$) and 1.3 log_{10} $TCID_{50}$/mg

https://doi.org/10.1038/s41467-024-52071-5

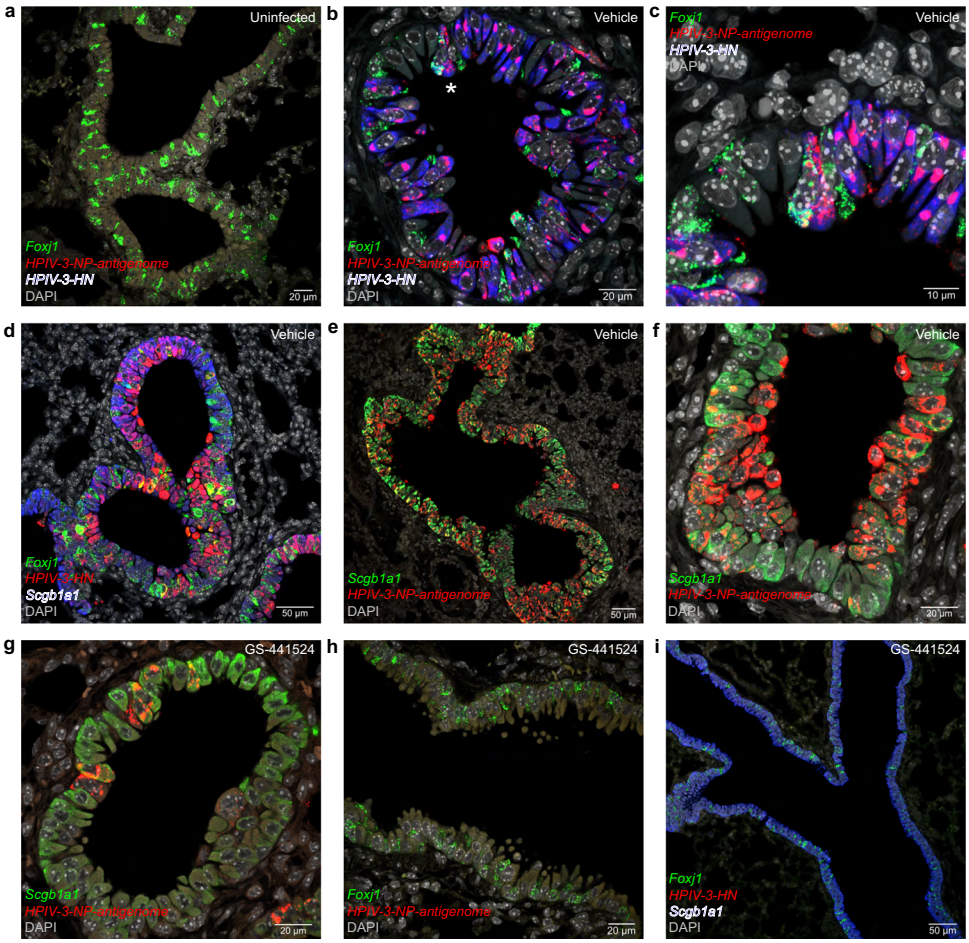

Fig. 4 | Visualizing *HPIV-3* RNA species in vehicle-treated vs. GS-441524-treated AG129 mice. Confocal images of sections through lung samples. Multiplex fluorescence with double or triple RNAscope. The name of a viral RNA species that is a target for an RNAscope probe, yielding puncta, is in italics. *HPIV-3-NP-antigenome* puncta visualize positive-sense viral RNA species. DAPI serves as nuclear stain. **a** Uninfected, **b**–**f** vehicle-treated, **g**–**i** GS-441524-treated. **a** Transverse section through two adjacent bronchioles. The lumen of the bronchioles (the black spaces at the center) is devoid of cells. *Foxj1* is a marker for ciliated cells. As expected, there are no puncta for the *HPIV-3-HN* probe and for the *HPIV-3-NP-antigenome* probe in this uninfected mouse. **b** *HPIV-3-HN* puncta diffusely fill cells in the bronchiolar epithelium, and *HPIV-3-NP-antigenome* puncta are perinuclear. **c** An orthogonal projection of a z-stack of confocal slices of the region in (**b**) indicated with an asterisk. A cell at the center harbors both *Foxj1* puncta and *HPIV-3-NP-antigenome* puncta; these puncta appear yellow in overlay. **d** *Scgb1a1* is a marker for club cells in the bronchiolar epithelium. A great many cells in the epithelium of two adjacent bronchioles harbor *HPIV-3-HN* puncta, colocalizing with *Foxj1* puncta or *Scgb1a1* puncta within the same cells. **e**, **f** Numerous cells in the bronchiolar epithelium harbor *HPIV-3-NP-antigenome* puncta. **g** In contrast, very few cells (**g**) or no cells (**h**) in the bronchiolar epithelium harbor *HPIV-3-NP-antigenome* puncta. **i** There are no *HPIV-3-HN* puncta detectable in this larger field of view. The epithelium is referred to as bronchiolar epithelium, as the sections were made through parts of the lungs that are located peripherally. Numbers of biological replicates: **a**, $n = 2$; **b**–**i**, $n = 3$.

lung sample ($p = 0.0390$) in the −6 h and −1 h treatment groups, respectively (Fig. 6b). Consistently, this prophylaxis reduced HPIV-3 RNA by 1.1 $\log_{10}$ $TCID_{50}$ equivalent/mg lung sample ($p = 0.0392$) and 1.8 $\log_{10}$ $TCID_{50}$ equivalent/mg lung sample ($p = 0.0060$) in the −6 h and −1 h treatment groups, respectively (Fig. 6c). Thus, a single prophylactic treatment of GS-441524 resulted in inhibition of HPIV-3 replication in the lung.

HPIV-3-infected mice do not transmit the virus to sentinels

Finally, we explored whether HPIV-3 can be transmitted from experimentally infected AG129 mice to sentinel mice. Six AG129 mice were intranasally inoculated with HPIV-3 and at day 1 p.i., each index mouse was co-housed in a cage with a sentinel mouse for 2 days. The index mice were killed at day 3 p.i., and the sentinel mice were killed the following day (Fig. S4a). There was no significant weight loss in either group (Fig. S4b). No virus was detected in the lung of all sentinels, and minute amounts in the NPLT-washes of one sentinel (Fig. S4c). Taken together, HPIV-3-infected AG129 mice do not readily transmit the virus to other mice in this experimental context.

Discussion

HPIV-3 infection is an important cause of lower respiratory tract illnesses in vulnerable populations, including children under 5 years, the elderly, and immunocompromised individuals. There are no vaccines nor antiviral drugs for the prevention and treatment of infections with HPIV-3 or other HPIVs. We here report a robust small-animal model for HPIV-3 infection that may serve as a preclinical model for antiviral studies.

We explored the replication capacity of HPIV-3 in the airways of mice following intranasal inoculation. Among the five inbred strains of mice we studied, AG129 mice were clearly the most susceptible. We ascribe their susceptibility to the failure of activation of the interferon pathways, which play a crucial role in the host antiviral response against viruses[36]. AG129 mice lack a functional IFN α/β/γ immune response. HPIV-3 infection results in the production of type I and type II interferons[37], which inhibit HPIV-3 replication[38,39]. Conversely, the rapid clearance of HPIV-3 replication in mice such as C57BL/6 and BALB/c mice can likely be ascribed to an efficient interferon response. Interestingly a patient, exhibiting a complete deficiency of IFNγ

https://doi.org/10.1038/s41467-024-52071-5

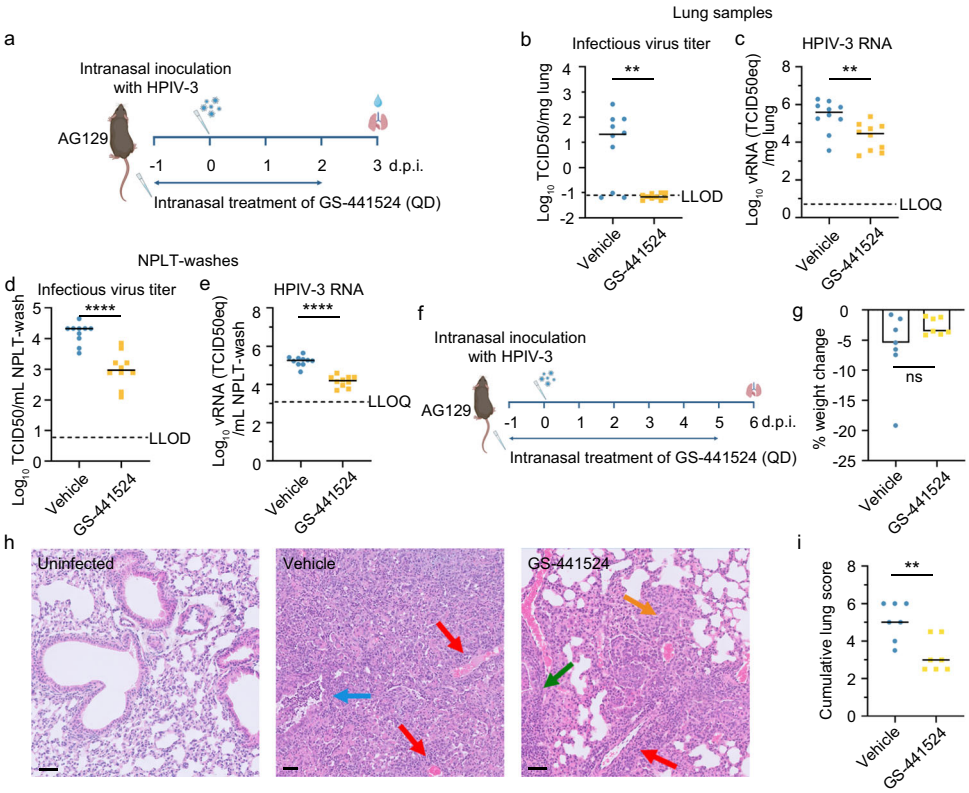

Fig. 5 | Intranasal treatment with GS-441524 of intranasally inoculated AG129 mice reduces viral loads in the lung and NPLT-washes and lung pathology. **a** Setup of the study. AG129 mice were intranasally treated once daily with either vehicle or GS-441524 (40 μL/mouse of a 30 mg/mL solution) from day −1 p.i. to day 2 p.i., and intranasally inoculated with 1.5×10^6 $TCID_{50}$ of HPIV-3 at day 0 p.i. Lung samples and NPLT-washes were collected at day 3 p.i. to measure viral loads. **b** Infectious virus titers are expressed as $\log_{10}$ $TCID_{50}$ per milligram of lung sample. **c** HPIV-3 RNA levels are expressed as $\log_{10}$ $TCID_{50}$ equivalent per milligram of lung sample. **d** Infectious virus titers are expressed as $\log_{10}$ $TCID_{50}$ per milliliter of NPLT-wash. **e** HPIV-3 RNA levels are expressed as $\log_{10}$ $TCID_{50}$ equivalent per milliliter of NPLT-wash. **b**–**e** LLOD presents the lower limit of detection. LLOQ presents the lower limit of quantification. Data are from two independent experiments with ten mice per group. Data were analyzed by the two-tailed Mann–Whitney *U* test. $^*p = 0.0312$, $^{**}p = 0.0071$, $^{****}p < 0.0001$. **f** Setup of the study. AG129 mice were intranasally treated once daily with either vehicle or GS-441524 (40 μL/mouse of a 30 mg/mL solution) starting from day −1 p.i. and continued for five consecutive days. The mice were intranasally inoculated with 1.5×10^6 $TCID_{50}$ of HPIV-3 at day 0 p.i. Lung samples were collected at day 6 p.i. for lung histopathology assessment. **g** Weight change at day 6 p.i. is presented as a percentage of the body weight at day −1 p.i., when treatment was started. **h** Representative H&E-stained images of the lung show bronchopneumonia (green arrow), perivascular inflammation (red arrows), peribronchial inflammation (blue arrow), and pneumocyte hyperplasia (orange arrow). The scale bar is 50 μm. **i** Cumulative severity scores of lungs of all infected mice. **g**, **i** Data are from one experiment, with seven mice per group. Data were analyzed with the two-tailed Mann–Whitney *U* test. ns nonsignificant, $^{**}p = 0.0070$. Individual data and median values (indicated by bars) are presented in all graphs. Source data are provided as a Source Data file. **a**, **f** were designed with BioRender.

responsiveness due to mutations in the IFNγ receptor gene, was reported to experience repeated viral infections including HPIV-3 within a short interval of 5 months and suffered from severe pneumonia complicated by respiratory failure requiring mechanical ventilation[40].

Whereas intranasal inoculation of AG129 mice with HPIV-3 did not result in observable disease or discomfort, post-mortem examination revealed viral replication and major respiratory pathology. We found that HPIV-3 replicated well in the upper and lower respiratory tracts of AG129 mice, with a rapid and sustained peak occurring from days 1 to 3 p.i. in the lung and a peak from days 1 to 5 p.i. in the NPLT-washes. By day 7 p.i., the infectious viruses were cleared completely from the lung and NPLT-washes. Lung pathology became prominent when viral replication was declining or undetectable. Despite the productive replication of HPIV-3 in the respiratory tracts of AG129 mice, we did not observe mouse-to-mouse transmission of the virus, probably due in part to a lack of clinical signs such as coughing or sneezing with subsequent spread of the virus. In ferrets as well, no horizontal transmission of the virus was demonstrated in a direct contact transmission experiment[15].

Infectious virus titers in the lung of AG129 mice appear comparable to those reported in cotton rats and are ~2 $\log_{10}$ higher than viral titers in the lung of hamsters[10], although a direct comparison is not possible. Viral loads in AG129 mice, however, are lower than those reported for patients[41–43]. Since we collected NPLT-washes rather than nasal swabs, nasopharyngeal swabs, or tracheal aspirates, a direct comparison is difficult. Additionally, as humans are the natural host, it may not be unexpected that viral loads are higher in humans. Active viral replication in the lung was further confirmed by using RNAscope, using a probe targeting positive-sense RNA of the nucleocapsid gene. Confocal imaging of sections stained with RNAscope and IHC indicated that HPIV-3 replicates in ciliated cells and club cells of the bronchiolar epithelium. We did not observe obvious colocalization of the virus with type I or type II pneumocytes in the alveolar wall. In an in vitro model of human pseudostratified mucociliary airway epithelium, HPIV-3 was shown to mainly infect ciliated cells[44]. HPIV-3 infection of a few type II pneumocytes was detected in lung organoids derived from human pluripotent stem cells[45]. It remains to be demonstrated whether or not HPIV-3 has a tropism for pneumocytes in the human lung. In ferrets, the virus was proposed to target type I and type II pneumocytes[15].

HPIV-3-infected AG129 mice developed peribronchial inflammation, perivascular inflammation, bronchopneumonia, and hyperplasia of pneumocytes. These features of bronchiolitis and pneumonia are

https://doi.org/10.1038/s41467-024-52071-5

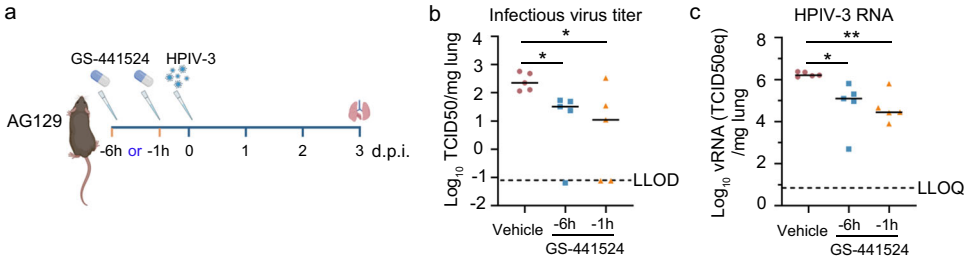

Fig. 6 | A single intranasal prophylactic dose of GS-441524 in AG129 mice intranasally inoculated with HPIV-3 reduces viral loads in the lung. a Setup of the study. AG129 mice were administrated intranasally with a single dose of GS-441524 (40 μL/mouse of a 30 mg/mL solution) at 6 or 1 h pre-infection, and then intranasally inoculated with 1.5×10^6 $TCID_{50}$ of HPIV-3. Lung samples were collected at day 3 p.i. to measure viral loads. **b** Infectious virus titers are expressed as log_{10} $TCID_{50}$ per milligram of lung sample. LLOD presents the lower limit of detection. **c** HPIV-3 RNA levels are expressed as log_{10} $TCID_{50}$ equivalent per milligram of lung sample. Data are from one experiment with five mice per group. Data were analyzed with the Kruskal–Wallis with Dunn's multiple comparisons test. $^*p = 0.0390$ (**b**), $^*p = 0.0392$ (**c**), $^{**}p = 0.0060$. Individual data and median values (indicated by bars) are presented in all graphs. Source data are provided as a Source Data file. **a** was designed with BioRender.

also seen in HPIV-3-infected patients[1]. HPIV-3-infected cotton rats present with bronchiolitis and interstitial pneumonia, but the pathological changes vary between the two cotton rat strains used[11]. HPIV-3-infected ferrets present with viral infection of the lungs but with minimal histological abnormalities[15]. HPIV-3-infected hamsters develop only mild inflammation and mild interstitial pneumonia[10]. HPIV-3-infected guinea pigs display hyperreactivity of the trachea but there is little information on viral replication in their respiratory tract[16–18,46]. HPIV-3-infected newborn lambs present with bronchointerstitial pneumonia characterized by bronchiolar hyperplasia and severe diffuse infiltration of macrophages in alveolar septae[9].

To seek further evidence that HPIV-3 indeed replicates in the respiratory tracts of AG129 mice, we explored whether the antiviral agent GS-441524, the parent nucleoside of remdesivir, can reduce viral replication in the respiratory tracts. Intracellularly, GS-441524 is converted to its 5′-triphosphate metabolite that inhibits the viral RNA-dependent RNA polymerase of coronaviruses and a number of other viruses/virus families including paramyxoviruses[27,35,47–50]. Obeldesivir (GS-5245), an oral prodrug with enhanced GS-441524 bioavailability, is currently in phase 3 clinical trials[51–53]. In the lung of HPIV-3-infected AG129 mice treated with oral doses of GS-441524, infectious virus titers were markedly reduced to even undetectable levels, and levels of HPIV-3 RNA were significantly reduced. Additionally, virtually no infected cells were detected in the respiratory tract by means of RNAscope. A single oral solution administration of 24 mg/kg GS-441524 (which is about half the efficacious dose of 50 mg/kg) given to uninfected mice, yielded a daily exposure ($AUC_{(0-24\,h)}$) of 13,100 ng h/mL (Fig. S5). Assuming proportional increases in plasma exposures, the projected estimates following 50 mg/kg, twice-a-day (BID) administrations to mice would yield an $AUC_{(0-24\,h)}$ value of 56,500 ng h/mL. This was roughly twice the plasma GS-441524 exposures that were achieved in humans following oral administration of a 350 mg BID regimen of obeldesivir[54]. These results support additional studies to establish the dose-dependent efficacy of oral obeldesivir treatment in this model.

Additionally, intranasal doses of GS-441524 decreased viral loads in the NPLT-washes as well as in the lung. Remarkably, even a single prophylactic intranasal dose at 6 or 1 h before infection yielded an antiviral effect. Together, these observations lend further support for our findings that HPIV-3 replicates well in the respiratory tract of AG129 mice. The finding that oral dosing (unlike intranasal dosing) did not reduce viral replication in the NPLT-washes may be explained by insufficient concentrations of the drug reaching the nasal epithelium.

There are no drugs approved for the treatment of severe infections with any of the four HPIVs. The use of ribavirin, dosed either aerosolized or orally, with or without intravenous gamma globulin, has been reported in small and uncontrolled series and in case reports of immunocompromised patients with severe HPIV-3 infections. The therapeutic effect varies, from no effect to a decrease in mortality and improvement of symptoms[55,56]. Additionally, in a few cases, the patients had to discontinue the treatment due to adverse effects, such as anemia[57]. Thus, ribavirin is certainly not an ideal drug for the treatment of infections by HPIVs. Severe HPIV infections may develop in the elderly and patients with underlying chronic conditions and may even be fatal in immunocompromised patients, in particular in recipients of a hematopoietic stem cell transplant and in children with severe combined immunodeficiency disease syndrome[40,55,56,58,59]. Since remdesivir has been approved for the treatment of SARS-CoV-2 infection and is safe and well tolerated, we propose that it (or obeldesivir) should be considered for the treatment of HPIV infections. Viral replication in immunocompromised patients may well be prolonged, such that antiviral efficacy can still be expected even when treatment is started relatively late. In immunocompetent patients at high or higher risk, such as those with underlying cardiac or lung disease, viral replication in the respiratory tract may be transient, (similar to our mouse model) such that early start of antiviral treatment might be of key importance.

In conclusion, we established a robust and convenient HPIV-3 infection model in AG129 mice that mimics, to some extent, the HPIV-3-induced bronchiolitis and (broncho)pneumonia that is observed in humans. This model will be instrumental for developing therapeutic and prophylactic modalities against this virus. We demonstrated in this model the therapeutic potential of GS-441524 and its prodrug forms for the treatment of HPIV-3.

Methods

Animals

C57BL/6 mice were purchased from Janvier Laboratories. Ifnar−/− mice (C57BL/6J mice with a knockout in the IFNα receptor 1 gene) and AG129 mice (129/Sv mice with knockouts in both IFNα/β and IFNγ receptor genes) were bred in-house. Ifnar−/− breeding pairs were a generous gift of Dr. Claude Libert, IRC/VIB, University of Ghent, Belgium. Breeding couples of AG129 mice were purchased from Marshall BioResources. The specific pathogen-free status of the mice is regularly checked at the KU Leuven animal facility of the Rega Institute. Inoculation was performed in 6–8 week-old female C57BL/6 and Ifnar −/− mice and in 8–12 week-old female and male AG129 mice. Mice were housed in individually ventilated isolator cages (IsoCage N Biocontainment System, Tecniplast) at a temperature of 21 °C, humidity of 55%, and subjected to 12:12 dark/light cycles. They had access to food and water *ad libitum*, and their cages were enriched with cotton and cardboard play tunnels for mice. Housing conditions and experimental procedures were approved by the Ethical Committee Dierproeven of KU Leuven (License P099/2022), following institutional guidelines approved by the Federation of European Laboratory Animal Science

Associations. The animal work was conducted under Biosafety Level 2 conditions. There was no preference for the gender of the mice used in all experiments; the choice of sex depended on their availability. Mice were anesthetized by inhalation with isoflurane before infection and killed by administering 100 μL of intraperitoneal Dolethal before sample collection. Mice were monitored daily for any signs of disease.

Cells and virus

LLC-MK2 cells (rhesus monkey kidney, ATCC, CCL-7) were cultured in DMEM/F-12 medium supplemented with 10% fetal bovine serum and 1.5% HEPES at 37 °C in a 5% CO_2 incubator. Endpoint titrations were performed using medium containing 2% fetal bovine serum instead of 10%.

HPIV-3, designated isolate 10-012854, was obtained from a nasopharyngeal wash collected from a patient in March 2010 at University Medical Center in Utrecht, The Netherlands. The isolate was propagated for 3 passages in LLC-MK2 cells to generate the virus stock used for inoculation, which has a titer of 3.8×10^7 $TCID_{50}$/mL. Iketani et al. reported 9 mutations emerging in the *HN* gene of cultured isolates: L239F, P241L, R242K, H552Q, S554N, L555S, L555F, N556D, and T557I, and described that HPIV-3 isolation in cell lines resulted in a loss of viral entry properties required for fitness in humans[60]. We did not observe any of these amino acid changes in the genome of the virus stock used for inoculation. The full genome of isolate 10-012854 is available in GenBank under accession number PP909812.

Compounds

GS-441524 was purchased from Excenen Pharmatech Co., Ltd. (China) and formulated as 15 mg/mL or 30 mg/mL stocks in 30% PEG_{400} (Sigma) in PBS containing 1% DMSO.

HPIV-3 infection of mouse strains

Mice were anesthetized with isoflurane and inoculated intranasally with 40 μL of medium containing 1.5×10^6 $TCID_{50}$ HPIV-3-isolate 10-012854 at day 0. Mice were monitored daily for weight changes and clinical signs. At indicated time points, mice were killed by intraperitoneal injection of 100 μL Dolethal. Nasal-pharyngeal-laryngeal-tracheal washes and lung samples were collected for quantification of infectious virus titers. A portion of the lung was fixed in 4% formaldehyde for histological analysis.

Treatment regimen

In oral treatment assays, AG129 mice were administered either vehicle ($n = 12$) or 50 mg/kg GS-441524 ($n = 12$) twice daily (BID) from day −1 to the endpoint. For intranasal treatment assays, AG129 mice were administered either vehicle ($n = 11$) or GS-441524 (40 μL/mouse of a 30 mg/mL solution) ($n = 11$) once daily (QD) from day −1 to the endpoint. At day 0, mice were anesthetized with isoflurane and intranasally inoculated with 40 μL of medium containing 1.5×10^6 $TCID_{50}$ HPIV-3-isolate 10-012854. At day 3 p.i., mice were killed to collect nasal-pharyngeal-laryngeal-tracheal washes and lung samples for quantification of infectious virus titers and HPIV-3 RNA levels. At day 6 p.i., mice were killed to collect lung samples, and a portion of the lung was fixed in 4% formaldehyde for subsequent histological analysis.

Sample collection

Lung samples were collected and homogenized using bead disruption (Precellys) in 400 μL medium, followed by centrifugation (10,000 × *g*, 5 min) to pellet cell debris. The supernatant was then processed for endpoint virus titration. Nasal-pharyngeal-laryngeal-tracheal washes were collected with the following procedure. The skin surrounding the trachea of freshly killed mice was removed to expose the muscle surrounding the trachea. A small incision was made in the muscle to further expose the trachea. A small incision was made in the trachea and a catheter was inserted. Then, 400 μL of PBS was injected into the catheter using a syringe, and washes were collected from the nostrils. This washing procedure was repeated twice. The washes were then processed for endpoint virus titration.

Endpoint virus titration assay

The endpoint virus titration was conducted on LLC-MK2 cells in 96-well plates. Cytopathic effects induced by HPIV-3 were observed and scored under the microscope. Viral titers were calculated using the Reed and Muench method and expressed as the $TCID_{50}$ per milligram of lung sample or per milliliter of NPLT-wash.

RT-qPCR

RT-qPCR was conducted on a LIGHTcycler96 platform (Roche) using the iTaq universal probes one-step RT-qPCR KIT (Bio-Rad, Cat#1725141). The primers targeting the *HN* gene of HPIV-3 encoding hemagglutinin-neuraminidase were forward primer 5′-*TGATGAAAGATCAGATTATGCAT*-3′ and reverse primer 5′-*CCAGGACACCCAGTTGTG*-3′. The probe used was 5′-56-FAM/*TGGACCAGG*/ZEN/*GATATACTACAAAGGCAAAATAATAT TTCTC*/3IABkFQ/-3′. The primers and probe were purchased from Integrated DNA Technologies, Inc. Equivalent standard serial dilutions of the HPIV-3 virus stock were employed to quantify viral RNA levels per milligram of lung sample or per milliliter of NPLT-wash.

Histology

Lung samples were fixed overnight in 4% formaldehyde and embedded in paraffin. Tissue sections (5 μm) were stained with H&E and scored blindly for lung damage by an expert pathologist. The 5 parameters, congestion, intra-alveolar hemorrhages, intra-alveolar edema, apoptotic bodies in the bronchus wall, and perivascular edema, were scored 0 or 1 for absent or present. The 3 parameters, perivascular inflammation, peribronchial inflammation, and vasculitis were scored on a scale of 0 to 3, depending on the number of inflammatory cells. Bronchopneumonia was scored on a scale of 0–3 depending on the extent of the pathology: 1 is ≤40%, 2 is between 41% and 60%, and 3 is ≥61% of the affected lung area[61]. A cumulative score was calculated by summing the scores of each parameter. The higher the number, the worse the pathology. The max score is 17. The epithelium in the images of Figs. 2 and 4 is referred to as “bronchiolar epithelium”, as the sections were made through parts of the lungs that are located peripherally.

RNAscope probes

Probes custom-designed by Advanced Cell Diagnostics against the gene encoding HPIV-3 nucleocapsid protein are: V-V-HPIV3-NP-C1 (Cat#1268201-C1), V-V-HPIV3-NP-C2 (Cat#1268201-C2), and reverse complement version V-V-HPIV3-NP-sense-C3 (Cat#1268848-C3). These custom-designed probes are commercially available. Catalog probes purchased from Advanced Cell Diagnostics are: V-HPIV3-HN-C1 (Cat#1223331-C1), Mm-Foxj1-C2 (Cat#317091-C2), Mm-Foxj1-C3 (Cat#317091-C3), Mm-Scgb1a1-C2 (Cat#420351-C2), Mm-Scgb1a1-C3 (Cat#420351-C3), Mm-Sftpc-C4 (Cat#314101-C4), Mm-Sftpb-No-XHs-C2 (Cat#539421-C2), and Mm-Ager-O1 (Cat#550791-C1).

RNAscope in situ hybridization

The RNAscope fluorescence manual assay was performed on lung FFPE sections at 5 μm thickness. Multiplex hybridization was detected with the Multiplex Fluorescent Detection Kit v2 (Advanced Cell Diagnostics, Cat# 323110) according to the manufacturer’s protocol and as previously described[30,31]. Briefly, slides were baked at 60 °C for 1 h, followed by deparaffinization in Xylene (Leica Biosystems, Cat# 3803665EG) and 100% ethanol wash. Sections were incubated in hydrogen peroxide for 15 min at room temperature. Tissue pretreatment was performed by steaming in target retrieval reagent (Advanced Cell Diagnostics, Cat#322000) for 30 min followed by incubation in Protease Plus (Advanced Cell Diagnostics, Cat#322330) at 40 °C for

30 min. RNAscope probes were hybridized at 40 °C for 2 h. Signal amplification steps were performed, followed by the development of specific HRP channels with different fluorophores assigned to each channel. The C4 channel probe was developed with the RNAscope 4-Plex Ancillary Kit (Advanced Cell Diagnostics, Cat#323120). Fluorophore dyes used were Opal 520 (Akoya Biosciences, Cat#FP1487001KT), Opal 570 (Akoya Biosciences, Cat#FP1488001KT), and Opal 690 (Akoya Biosciences, Cat#FP1497001KT). DAPI (Thermo Fisher Scientific, Cat#D1306) served as a nuclear stain. Slides were mounted in Mount Solid antifade (Abberior, Cat#MM-2011-2X15ML). Confocal images were taken on a Zeiss LSM 800.

Immunohistochemistry (IHC)

IHC for codetection of RNA and protein was performed for Cytokeratin 8 immunoreactivity after the final HRP blocker step. Slides were blocked in 10% donkey serum (Sigma-Aldrich, Cat#S30-100ML) in 0.1% Triton in PBS at room temperature for 1 h. Primary antibody Krt8, clone TROMA-1 (Sigma-Aldrich, Cat#MABT329) raised in rat, was diluted at 1:200 in 2% donkey serum in 0.1% Triton/PBS and incubated at 4 °C overnight. Slides were then washed in 0.1% Triton for three times for 5 min in PBS, followed by incubation with Alexa Fluor Plus 647 donkey anti-rat (Thermo Fisher Scientific, Cat#A48272) at 1:500 in 2% normal donkey serum in 0.1% Triton/PBS at room temperature for 1 h.

Transmission

Index AG129 mice aged 8–12 weeks ($n = 6$) were anesthetized with isoflurane and intranasally inoculated with 40 μL of medium containing 1.5×10^6 $TCID_{50}$ HPIV-3-isolate 10-012854 at day 0. On the morning of day 1 p.i., each index AG129 mouse was co-housed with an uninfected contact (sentinel) AG129 mouse ($n = 6$) in a cage. Co-housing continued for 2 days, when the index mice were killed, and the sentinel mice were killed the following day. Lung samples were collected.

Pharmacokinetic study

Mouse pharmacokinetic studies were performed at Covance Laboratories (LabCorp Drug Development) as described previously[62]. Briefly, female BALB/c ($n = 8$) were administered GS-441524 (same formulation as used previously[27]) at 24 mg/kg by oral gavage, and plasma concentrations (ng/mL) were quantitated at select timepoints over 24 h.

Statistics

GraphPad Prism (GraphPad Software, Inc.) was used to perform statistical analysis. Statistical significance was determined using the nonparametric Kruskal–Wallis test with Dunn's multiple comparisons test for multiple comparisons or the Mann–Whitney U test for pairwise comparisons. p values of <0.05 were considered significant. Exact p values are provided except for p values smaller than 0.0001, which are presented as $p < 0.0001$. All measurements were taken from distinct samples.

Ethics

Housing conditions and experimental procedures were with the approval and under the guidelines of the Ethical Committee Dierproeven of KU Leuven (License P099/2022).

Reporting summary

Further information on research design is available in the Nature Portfolio Reporting Summary linked to this article.

Data availability

All data generated and analyzed in this paper are included in this article. The deep sequencing data of the full genome of the isolate used in this study are available in GenBank under accession number PP909812. Additional imaging data related to the RNAscope analysis are available from the corresponding author upon request. Source data are provided with this paper.

References

1. Branche, A. R. & Falsey, A. R. Parainfluenza virus infection. *Semin. Respir. Crit. Care Med.* **37**, 538–554 (2016).
2. Pan, Y. et al. Human parainfluenza virus infection in severe acute respiratory infection cases in Beijing, 2014-2016: a molecular epidemiological study. *Influenza Other Respir. Viruses* **11**, 564–568 (2017).
3. Ben-Shimol, S., Landau, D., Zilber, S. & Greenberg, D. Parainfluenza virus type 3 outbreak in a neonatal nursery. *Clin. Pediatr.* **52**, 866–870 (2013).
4. Maeda, H., Haneda, K. & Honda, Y. Parainfluenza virus type 3 outbreak in a neonatal intensive care unit. *Pediatr. Int.* **59**, 1219–1222 (2017).
5. Henrickson, K. J. Parainfluenza viruses. *Clin. Microbiol. Rev.* **16**, 242–264 (2003).
6. Morein, B., Sharp, M., Sundquist, B. & Simons, K. Protein subunit vaccines of parainfluenza type 3 virus: immunogenic effect in lambs and mice. *J. Gen. Virol.* **64**, 1557–1569 (1983).
7. Senchi, K., Matsunaga, S., Hasegawa, H., Kimura, H. & Ryo, A. Development of oligomannose-coated liposome-based nasal vaccine against human parainfluenza virus type 3. *Front. Microbiol.* **4**, 346 (2013).
8. Stewart-Jones, G. B. E. et al. Structure-based design of a quadrivalent fusion glycoprotein vaccine for human parainfluenza virus types 1-4. *Proc. Natl. Acad. Sci. USA* **115**, 12265–12270 (2018).
9. Garg, R. et al. Maternal vaccination with a novel chimeric glycoprotein formulated with a polymer-based adjuvant provides protection from human parainfluenza virus type 3 in newborn lambs. *Antivir. Res.* **162**, 54–60 (2019).
10. Glezen, W. P. & Fernald, G. W. Effect of passive antibody on parainfluenza virus type 3 pneumonia in hamsters. *Infect. Immun.* **14**, 212–216 (1976).
11. Porter, D. D., Prince, G. A., Hemming, V. G. & Porter, H. G. Pathogenesis of human parainfluenza virus 3 infection in two species of cotton rats: Sigmodon hispidus develops bronchiolitis, while Sigmodon fulviventer develops interstitial pneumonia. *J. Virol.* **65**, 103–111 (1991).
12. Ambrose, M. W. et al. Evaluation of the immunogenicity and protective efficacy of a candidate parainfluenza virus type 3 subunit vaccine in cotton rats. *Vaccine* **9**, 505–511 (1991).
13. Ottolini, M. G., Porter, D. D., Blanco, J. C. & Prince, G. A. A cotton rat model of human parainfluenza 3 laryngotracheitis: virus growth, pathology, and therapy. *J. Infect. Dis.* **186**, 1713–1717 (2002).
14. Jones, B. G., Hayden, R. T. & Hurwitz, J. L. Inhibition of primary clinical isolates of human parainfluenza virus by DAS181 in cell culture and in a cotton rat model. *Antivir. Res.* **100**, 562–566 (2013).
15. Rijsbergen, L. C. et al. Modeling infection and tropism of human parainfluenza virus type 3 in ferrets. *mBio* **13**, e0383121 (2021).
16. Kudlacz, E. M., Baugh, L. E., Porter, W. P., Kenny, M. T. & Farrell, A. M. A time-course study of airway hyperresponsiveness in conscious parainfluenza virus type 3-infected guinea pigs. *Lab Anim. Sci.* **43**, 445–453 (1993).
17. Ye, X. M., Zhong, N. S., Liu, C. L. & Chen, R. C. Cough reflex sensitivity is increased in guinea pigs with parainfluenza virus infection. *Exp. Lung Res.* **37**, 186–194 (2011).
18. Zaccone, E. J. et al. Parainfluenza 3-induced cough hypersensitivity in the guinea pig airways. *PLoS ONE* **11**, e0155526 (2016).
19. Durbin, A. P., Elkins, W. R. & Murphy, B. R. African green monkeys provide a useful nonhuman primate model for the study of human parainfluenza virus types-1, -2, and -3 infection. *Vaccine* **18**, 2462–2469 (2000).
20. van Wyke Coelingh, K. L., Winter, C. C., Tierney, E. L., London, W. T. & Murphy, B. R. Attenuation of bovine parainfluenza virus type 3 in nonhuman primates and its ability to confer immunity to human

parainfluenza virus type 3 challenge. *J. Infect. Dis.* **157**, 655–662 (1988).
21. Durbin, A. P., Wyatt, L. S., Siew, J., Moss, B. & Murphy, B. R. The immunogenicity and efficacy of intranasally or parenterally administered replication-deficient vaccinia-parainfluenza virus type 3 recombinants in rhesus monkeys. *Vaccine* **16**, 1324–1330 (1998).
22. Garg, R. et al. A chimeric glycoprotein formulated with a combination adjuvant induces protective immunity against both human respiratory syncytial virus and parainfluenza virus type 3. *Antivir. Res.* **158**, 78–87 (2018).
23. van den Broek, M. F., Müller, U., Huang, S., Zinkernagel, R. M. & Aguet, M. Immune defence in mice lacking type I and/or type II interferon receptors. *Immunol. Rev.* **148**, 5–18 (1995).
24. Meng, T. & Kwang, J. Attenuation of human enterovirus 71 high-replication-fidelity variants in AG129 mice. *J. Virol.* **88**, 5803–5815 (2014).
25. Kaptein, S. J. F. et al. A pan-serotype dengue virus inhibitor targeting the NS3-NS4B interaction. *Nature* **598**, 504–509 (2021).
26. Baldon, L. V. R. et al. AG129 mice as a comprehensive model for the experimental assessment of mosquito vector competence for arboviruses. *Pathogens* **11**, 879 (2022).
27. Cox, R. M. et al. Oral prodrug of remdesivir parent GS-441524 is efficacious against SARS-CoV-2 in ferrets. *Nat. Commun.* **12**, 6415 (2021).
28. Wang, F. et al. RNAscope: a novel in situ RNA analysis platform for formalin-fixed, paraffin-embedded tissues. *J. Mol. Diagn.* **14**, 22–29 (2012).
29. Ceulemans, L. J. et al. Persistence of SARS-CoV-2 RNA in lung tissue after mild COVID-19. *Lancet Respir. Med.* **9**, e78–e79 (2021).
30. Khan, M. et al. Visualizing in deceased COVID-19 patients how SARS-CoV-2 attacks the respiratory and olfactory mucosae but spares the olfactory bulb. *Cell* **184**, 5932–5949.e5915 (2021).
31. Khan, M. et al. Anatomical barriers against SARS-CoV-2 neuroinvasion at vulnerable interfaces visualized in deceased COVID-19 patients. *Neuron* **110**, 3919–3935.e3916 (2022).
32. Van Slambrouck, J. et al. Visualising SARS-CoV-2 infection of the lung in deceased COVID-19 patients. *EBioMedicine* **92**, 104608 (2023).
33. Clijsters, M. et al. Protocol for postmortem bedside endoscopic procedure to sample human respiratory and olfactory cleft mucosa, olfactory bulbs, and frontal lobe. *STAR Protoc.* **5**, 102831 (2024).
34. Administration, U. S. F. D. FDA Approves First Treatment for COVID-19. https://www.fda.gov/news-events/press-announcements/fda-approves-first-treatment-covid-19 (2020).
35. Lo, M. K. et al. GS-5734 and its parent nucleoside analog inhibit Filo-, Pneumo-, and Paramyxoviruses. *Sci. Rep.* **7**, 43395 (2017).
36. Dalskov, L., Gad, H. H. & Hartmann, R. Viral recognition and the antiviral interferon response. *EMBO J.* **42**, e112907 (2023).
37. Lewandowska-Polak, A. et al. Human parainfluenza virus type 3 (HPIV3) induces production of IFNγ and RANTES in human nasal epithelial cells (HNECs). *J. Inflamm.* **12**, 16 (2015).
38. Choudhary, S., Gao, J., Leaman, D. W. & De, B. P. Interferon action against human parainfluenza virus type 3: involvement of a novel antiviral pathway in the inhibition of transcription. *J. Virol.* **75**, 4823–4831 (2001).
39. Rabbani, M. A., Ribaudo, M., Guo, J. T. & Barik, S. Identification of interferon-stimulated gene proteins that Inhibit human parainfluenza virus type 3. *J. Virol.* **90**, 11145–11156 (2016).
40. Dorman, S. E. et al. Viral infections in interferon-gamma receptor deficiency. *J. Pediatr.* **135**, 640–643 (1999).
41. Piralla, A., Percivalle, E., Di Cesare-Merlone, A., Locatelli, F. & Gerna, G. Multicluster nosocomial outbreak of parainfluenza virus type 3 infection in a pediatric oncohematology unit: a phylogenetic study. *Haematologica* **94**, 833–839 (2009).
42. Lefeuvre, C. et al. Frequent lower respiratory tract disease in hematological patients with parainfluenza virus type 3 infection. *J. Med. Virol.* **93**, 6371–6376 (2021).
43. Greninger, A. L. et al. Human parainfluenza virus evolution during lung infection of immunocompromised individuals promotes viral persistence. *J. Clin. Invest.* **131**, e150506 (2021).
44. Zhang, L. et al. Infection of ciliated cells by human parainfluenza virus type 3 in an in vitro model of human airway epithelium. *J. Virol.* **79**, 1113–1124 (2005).
45. Porotto, M. et al. Authentic modeling of human respiratory virus infection in human pluripotent stem cell-derived lung organoids. *mBio* **10**, e00723-19 (2019).
46. Mascoli, C. C., Gower, T. A., Capilupo, F. A. & Metzgar, D. P. Further studies on the neonatal ferret model of infection and immunity to and attenuation of human parainfluenza viruses. *Dev. Biol. Stand.* **33**, 384–390 (1976).
47. Agostini, M. L. et al. Coronavirus susceptibility to the antiviral remdesivir (GS-5734) is mediated by the viral polymerase and the proofreading exoribonuclease. *mBio* **9**, e00221-18 (2018).
48. Yan, V. C. & Muller, F. L. Advantages of the parent nucleoside GS-441524 over remdesivir for Covid-19 treatment. *ACS Med. Chem. Lett.* **11**, 1361–1366 (2020).
49. Amirian, E. S. & Levy, J. K. Current knowledge about the antivirals remdesivir (GS-5734) and GS-441524 as therapeutic options for coronaviruses. *One Health* **9**, 100128 (2020).
50. Li, Y. et al. Remdesivir metabolite GS-441524 effectively inhibits SARS-CoV-2 infection in mouse models. *J. Med. Chem.* **65**, 2785–2793 (2022).
51. Martinez, D. R. et al. Efficacy of the oral nucleoside prodrug GS-5245 (Obeldesivir) against SARS-CoV-2 and coronaviruses with pandemic potential. *bioRxiv* https://doi.org/10.1101/2023.06.27.546784 (2023).
52. Mackman, R. L. et al. Discovery of GS-5245 (Obeldesivir), an oral prodrug of nucleoside GS-441524 that exhibits antiviral efficacy in SARS-CoV-2-infected African green monkeys. *J. Med. Chem.* **66**, 11701–11717 (2023).
53. Medicine, U. S. N. L. O. Study of obeldesivir in nonhospitalized participants with COVID-19 (OAKTREE). https://classic.clinicaltrials.gov/ct2/show/NCT05715528 (2023).
54. Pitts, J. Efficacy in multiple SARS-CoV-2 animal models supports phase 3 dose selection for obeldesivir. *Open Forum Infect. Dis.* https://doi.org/10.1093/ofid/ofad500.608 (2023).
55. Casey, J., Morris, K., Narayana, M., Nakagaki, M. & Kennedy, G. A. Oral ribavirin for treatment of respiratory syncitial virus and parainfluenza 3 virus infections post allogeneic haematopoietic stem cell transplantation. *Bone Marrow Transplant.* **48**, 1558–1561 (2013).
56. Stamouli, M. et al. Oral ribavirin is a highly effective treatment for lower respiratory tract infections due to respiratory syncytial virus or parainfluenza after allogeneic stem cell transplantation. *Bone Marrow Transplant.* **56**, 511–513 (2021).
57. Kwak, E., Abdel-Massih, R., Crespo, M., Pilewski, J. & Nguyen, M. Oral ribavirin for treatment of respiratory viral infection in lung transplant recipients.: Abstract# D2407. *Transplantation* **98**, 775 (2014).
58. Frank, J. A. Jr., Warren, R. W., Tucker, J. A., Zeller, J. & Wilfert, C. M. Disseminated parainfluenza infection in a child with severe combined immunodeficiency. *Am. J. Dis. Child* **137**, 1172–1174 (1983).
59. Falsey, A. R. Current management of parainfluenza pneumonitis in immunocompromised patients: a review. *Infect. Drug Resist.* **5**, 121–127 (2012).
60. Iketani, S. et al. Viral entry properties required for fitness in humans are lost through rapid genomic change during viral isolation. *mBio* **9**, e00898-18 (2018).

61. Gruber, A. D. et al. Standardization of reporting criteria for lung pathology in SARS-CoV-2-infected hamsters: what matters? *Am. J. Respir. Cell Mol. Biol.* **63**, 856–859 (2020).
62. Schäfer, A. et al. Therapeutic treatment with an oral prodrug of the remdesivir parental nucleoside is protective against SARS-CoV-2 pathogenesis in mice. *Sci. Transl. Med.* **14**, eabm3410 (2022).

Acknowledgements

We thank Stijn Hendrickx, Lindsey Bervoets, and Carolien De Keyzer for their excellent technical assistance. We thank the staff at the Rega animal facility of KU Leuven for technical assistance with the animal experiments. We also thank the staff at the Department of Translation Cell and Tissue Research at KU Leuven for histology sample processing and staining. This project was funded by EU PANVIPREP (Project number 101137229) and EU DURABLE (Project number 101102733). Y.L. was supported by the China Scholarship Council (Grant no. 202006380126). Figures were generated using BioRender.

Author contributions

J.N. acquired funding, designed the project, and wrote the manuscript. D.J. designed the project and assisted with the data analysis and manuscript writing. Y.L. designed and performed experiments, analyzed the data, made figures, and wrote the manuscript. P.M. designed the RNAscope and immunochemistry experiments and wrote the manuscript. M.K. designed and performed RNAscope and immunochemistry experiments, analyzed the data, made figures, and assisted with manuscript writing. B.W. performed the lung scoring and assisted with data analysis. F.C. isolated the HPIV-3 clinical isolate. D.B. and J.B. performed the pharmacokinetic study, analyzed the data, made the graph, and assisted with the manuscript writing. M.L. assisted with project design, data analysis, and manuscript writing. All authors have read and agreed with the content of the manuscript.

Competing interests

D.B. and J.B. are employees of Gilead Sciences which owns GS-441524. None of the other authors have any competing interests.

Additional information

Supplementary information The online version contains supplementary material available at https://doi.org/10.1038/s41467-024-52071-5.

Correspondence and requests for materials should be addressed to Johan Neyts.

Peer review information *Nature Communications* thanks Michael Lo and the other, anonymous, reviewers for their contribution to the peer review of this work. A peer review file is available.